AIMS Energy, 13(6): 1417–1431.
DOI: 10.3934/energy.2025053
Received: 29 August 2025
Revised: 28 October 2025
Accepted: 18 November 2025
Published: 24 November 2025

https://www.aimspress.com/journal/energy

Research article

Improving the efficiency of hydrogen storage in $LaNi_5$-based materials through cobalt modification

Arman Miniyazov[1,2], Mazhyn Skakov[1], Nuriya Mukhamedova[1,2,*], Mikhail Skopchenko[1], Ospan Oken[1], Aisara Sabyrtayeva[1], Igor Sokolov[1,2] and Anar Nassyrova[3]

[1] National Nuclear Centre RK, Kurchatov, 071100, Kazakhstan
[2] Department of Technical Physics and Heat Power Engineering, Shakarim University, Semey 071410, Kazakhstan
[3] S.Amanzholov East Kazakhstan University, Ust-Kamenogorsk, 070004, Kazakhstan

* **Correspondence:** E-mail: bakayeva@nnc.kz; Tel: +77753901070.

Abstract: This paper investigated the effect of cobalt on hydrogen storage in the intermetallic compound $LaNi_5$. Phase composition and hydrogen absorption properties of the $LaNi_5$–xCo_x system were analyzed using X-ray diffraction. The results demonstrated the retention of the hexagonal AB_5-type structure upon substitution of nickel atoms with cobalt atoms, accompanied by minor changes in lattice parameters and the formation of the $LaNi_4Co$ phase. Hydrogen absorption studies revealed an increase in the material's capacity to 1.9% and a reduction in the time required to reach 90% of the equilibrium concentration to 2–3 minutes. These findings indicate that cobalt modification is an effective method to enhance hydrogen storage efficiency.

Keywords: metal hydride; hydrogen storage; $LaNi_5$; cobalt; spark plasma sintering

1. Introduction

Hydrogen energy is one of the key areas in sustainable energy development, with the potential to facilitate the transition to a low-carbon economy. Unlike traditional carbon-based energy sources, the use of hydrogen as an energy carrier produces no CO_2 emissions; the only by-product of conversion in fuel cells is water [1–3]. This renders hydrogen energy a priority for countries striving to decarbonize industry, transport, and electricity generation. Amid the rapid advancement of hydrogen energy and

the increasing demand for environmentally friendly and efficient energy sources, the development of reliable and high-capacity hydrogen storage systems is becoming particularly relevant [4–6].

At the international level, hydrogen energy is being actively promoted through national programs and initiatives. Large countries such as Germany [7], Japan [8], and Austria [9] are implementing projects aimed at advancing hydrogen technologies and production. These examples demonstrate that hydrogen energy has moved beyond theoretical studies and laboratory experiments; it is now becoming an integral part of practical industrial solutions, playing a crucial role in the global energy transition toward cleaner and more sustainable sources.

A strategically important aspect of hydrogen energy is its use as a medium for energy storage. An additional benefit of hydrogen is its ability to serve as long-term energy storage, helping to balance seasonal and daily fluctuations in electricity generation from renewable sources. Through electrolysis powered by "green" electricity from solar and wind installations, hydrogen can effectively store excess electricity during periods of surplus and return it to the grid via fuel cells or turbo generators during demand peaks [10–12].

One of hydrogen's key advantages is its high specific combustion energy of ~140 MJ/kg [13], making it the most energy-dense fuel available. Consequently, hydrogen, with its high specific energy, is considered one of the most promising energy carriers of the future, although its storage and transportation pose several technical challenges [13–15]. Among the various hydrogen storage methods, such as compression, liquefaction, and chemical bonding, solid-phase storage in metal hydrides has attracted significant attention. Metal hydrides exhibit outstanding characteristics, with hydrogen storage densities in some cases exceeding that of liquid hydrogen on a volumetric basis. For instance, MgH_2 can store up to 0.11 kg H_2/L, compared to approximately 0.071 kg H_2/L for liquid hydrogen. Comparable values are observed in systems based on $LaNi_5H_6$, $TiFeH_2$, and other intermetallic compounds [16–18]. This storage method is distinguished by its high density, safety, and suitability for repeated cycling [19,20].

The formation of hydride phases in intermetallic compounds (IMCs) occurs through the penetration of hydrogen atoms into the interstices of the material's crystal lattice. This mechanism involves the adsorption of hydrogen molecules on the metal surface, their dissociation into atoms, and subsequent penetration into the lattice, resulting in the formation of a hydride phase at the interface between the metal and the hydride [21,22].

One of the most extensively studied and widely used materials for hydrogen storage is the intermetallic compound $LaNi_5$. $LaNi_5$ exhibits several unique properties: relatively low hydriding temperature and pressure, high hydrogen capacity (up to 1.4 wt.%), favorable absorption and desorption kinetics, and reversible processes [23,24]. Structurally, $LaNi_5$ belongs to the class of compounds with a hexagonal AB_5-type structure, in which hydrogen occupies interstitial sites to form the hydride $LaNi_5H_6$ [25]. According to numerous studies [26–29], the formation of the $LaNi_5H_6$ hydride phase is accompanied by lattice expansion (in which the unit cell volume increases by approximately 24% [30]) due to hydrogen atoms entering the interstices. During dehydrogenation, the crystal lattice returns to its original state; however, structural defects and dislocations accumulated during cycling remain, indicating irreversible microstructural damage. These defects can further contribute to the degradation of the hydrogen absorption properties [31].

To mitigate material degradation, alloying and modification of the $LaNi_5$ matrix with various elements, such as V, Ni, Al, Mn, and Co, are employed [32–34]. Cobalt (Co) is among the most effective elements for modifying the $LaNi_5$ matrix. Despite the chemical similarity between Co and Ni,

their behavior in alloys differs. Co has a lower electron density in its outer electron shells, rendering the Co–Ni bond softer. Consequently, Co reduces the alloy's hardness and enhances its plasticity, facilitating more effective relief of local stresses and preventing lattice damage during cyclic deformation [35,36].

Due to its larger atomic radius compared to Ni, Co modification results in an increase in the unit cell volume while maintaining the original crystal symmetry [36,37]. This expansion helps to reduce the plateau pressure and alleviate internal lattice stresses, as hydride phases form more readily in an expanded unit cell [38].

Notably, in $LaNi_{5-x}Co_x$ systems, a two-step plateau is often observed on pressure-composition-temperature (PCT) isotherms [32]. This behavior is attributed to the sequential occurrence of two phase transitions: $\alpha \rightarrow \beta$ (formation of the primary hydride phase) and $\beta \rightarrow \gamma$ (formation of a more hydrogen-saturated secondary hydride phase). The presence of Co stabilizes the γ-phase and increases the energy gap between the β- and γ-phases, leading to a clear distinction between these stages on the sorption curve.

Two-stage hydride formation has a beneficial effect on the long-term stability of the material: the redistribution of volume changes between two successive stages reduces local mechanical stresses, decreases particle pulverization, and mitigates capacity degradation during multiple hydrogenation–dehydrogenation cycles. The two-stage plateau effect is considered one of the factors contributing to the enhanced durability of Co-modified materials.

Overall, alloying and modifying the Ni sublattice with Co increases the alloy's resistance to local corrosion, thereby reducing the degradation of the active material during long-term operation [39,40]. It also lowers the equilibrium pressure and improves the thermodynamic stability of the hydride [40], accelerates the kinetics of both hydriding and dehydriding processes [37], and enhances cyclic stability by alleviating internal stresses within the structure [36]. Consequently, these effects can significantly increase cyclic stability, reduce self-discharge rates, and extend the service life of metal hydride electrodes. Furthermore, Co modification promotes the stabilization of triclinic phases and reduces deformation during charge–discharge cycles, which is crucial for long-term use [33]. For the past 10 years, the National Nuclear Center of the Republic of Kazakhstan has been conducting research aimed at improving hydrogen production technologies [41,42] and developing materials for hydrogen storage [43–46]. Particular attention is given to the study of the $LaNi_5$ system as an anode material for Ni-MH batteries [47,48].

It is hypothesized that modification of the $LaNi_5$ system with cobalt improves the structural and surface properties of the material, leading to enhanced hydrogen storage efficiency through increased absorption rates and hydrogen storage capacity.

Thus, understanding the effect of Co on the structure and properties of $LaNi_5$ is key to developing efficient next-generation hydrogen storage devices. This article discusses the mechanisms underlying the enhanced hydrogen storage efficiency in $LaNi_5$ systems substituted with Co, as well as the changes in crystal structure, thermodynamic, and kinetic characteristics of hydrides resulting from the application of spark plasma sintering (SPS) technology in material synthesis. The novelty of this work lies in its comprehensive study of the effects of Co substitution in the intermetallic compound $LaNi_5$ on the hydrogen-accumulating properties of the material, with a particular emphasis on the modification of thermodynamic and kinetic characteristics of hydrogen absorption and desorption.

2. Materials and methods

The subject of this study is the intermetallic LaNi system modified with the addition of Co. The Co addition was intended to modify the crystal lattice and enhance the hydrogen absorption characteristics of the material.

Powders of the initial metals—lanthanum (La), nickel (Ni), and cobalt (Co), each with 99.95% purity—were weighed in stoichiometric proportions of 20 wt.% La, 40 wt.% Ni, and 40 wt.% Co. These powders were subjected to MS using a Pulverisette 7 planetary ball mill. The milling process was conducted under an argon atmosphere at a rotational speed of 350 rpm for 8 hours, employing solid steel balls with a grinding ball-to-powder mass ratio (BPR) of 20:1 for sample LNC-1 and 30:1 for sample LNC-2. After milling, the powders were stored in sealed containers to prevent oxidation.

Bulk laboratory samples were fabricated using the spark plasma sintering (SPS) method on an ISKRA apparatus. The sintering process was carried out in vacuum conditions (up to 10^{-3} Pa) at a temperature of 1000 ± 50 °C and a pressure of 30 MPa for 5 minutes. The resulting sintered samples were cylindrical, with a diameter of 20 mm and a thickness of 5 ± 0.2 mm (Figure 1).

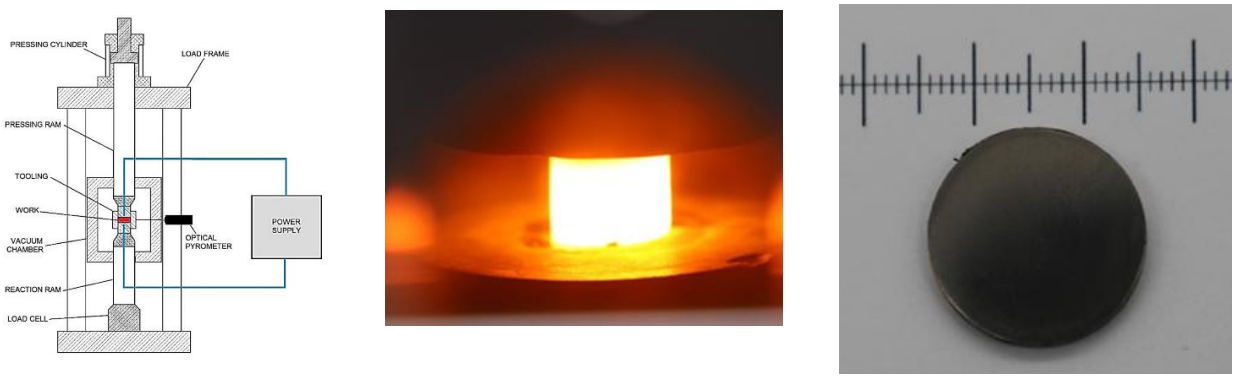

a) block diagram of the ISKRA installation.

b) sintering process

c) sintering process

Figure 1. Sintering scheme and process on the ISKRA installation.

Subsequent dispersion of the obtained sintered materials was carried out in a ball mill using an 80 mL jar and grinding balls with a diameter of 50 mm, made from tungsten carbide (material hardness of 89.7 HRA), which facilitated effective dispersion of the sintered materials. Dispersion was performed to increase the specific surface area for interaction with hydrogen, while preserving the structural characteristics obtained by SPS [46].

Phase composition was evaluated using X-ray diffraction (XRD) with a D6 Phaser diffractometer employing monochromatic Cu Kα radiation (λ = 0.15418 nm) over a 2θ range of 20–90°, with a step size Δ2θ of 0.013° and a counting time of 23.4 s per step. During data collection, the voltage and current were set at 40 kV and 30 mA, respectively, and the sample stage was rotated at 5 rpm. The diffraction patterns were analyzed using the dedicated DIFFRAC.EVA software, with reflex identification based on the PDF-4 Axiom 2025 database [49]. Phase identification was performed by assessing angular positions, phase intensities at different angles, and comparison of interplanar spacing data. Peak height and full width at half maximum (FWHM) were obtained via automated profile

analysis within the DIFFRAC.EVA software, applying the Voigt function [50]. For more detailed analysis, lattice parameters, microstrain (ε), and average crystallite size (D) were calculated using the Williamson–Hall method. Quantitative phase analysis was conducted by Rietveld refinement [51] of the XRD profile using the TOPAS 5 software package (Bruker AXS, Germany).

Hydrogen absorption characteristics were assessed by pressure-composition-temperature (PCT) manometric measurements using the automated H-Sorb system. Measurements were performed at 100 °C over a pressure range of 0–2 MPa. The following parameters were determined: maximum achievable hydrogen capacity (wt.% H_2), plateau pressures for hydriding/dehydriding, hysteresis between absorption and desorption, and saturation rate (t%).

3. Results and discussion

X-ray phase analysis

Based on the obtained X-ray phase analysis data and the calculated lattice parameters, an analysis of the phase composition and structural characteristics of the Co-modified samples after all technological processing stages was carried out. The overlaid diffraction patterns of samples LNC-1 and LNC-2 are presented in Figure 2.

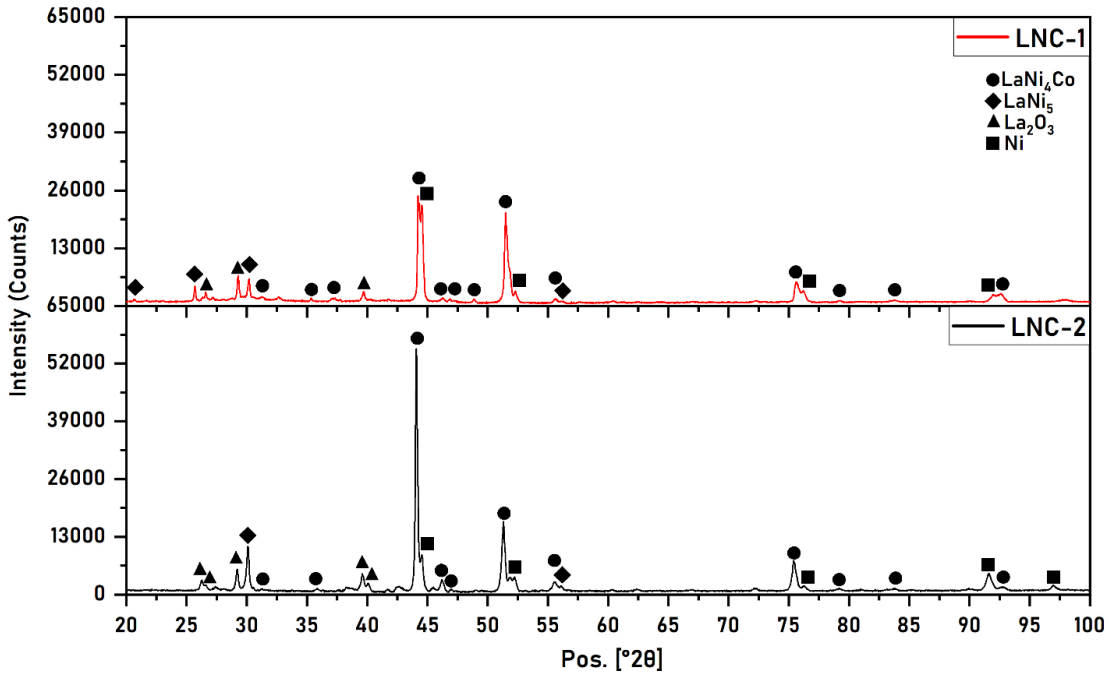

Figure 2. Overlay of diffraction patterns of samples LNC-1 and LNC-2 after dispersion.

It was established that the addition of Co to the matrix phase $LaNi_5$ results in the substitution of one nickel atom by cobalt, leading to the formation of the $LaNi_4Co$ phase. This substitution is possible due to the similar atomic radii and electronic configurations of Ni and Co, which allows Co to isomorphically enter the structure without significant distortion of the crystal lattice. Such partial substitution has a notable impact on the structural and functional properties of the resulting intermetallic compound. The studied samples exhibited an identical phase composition. For the detected inclusions, data on microstrain and quantitative phase content are presented in Table 1.

Table 1. Phase composition and structural parameters.

Sample	Phase	a (Å)	c (Å)	Weight fraction (%)	ε (%)	D_{avg} (nm)
LNC-1	$LaNi_4Co$	5.197	3.868	68.878 ± 0.9	0.11 ± 0.01	83.31
	$LaNi_5$	5.171	4.041	18.991 ± 1.2	0.18 ± 0.05	75.97
	Ni	3.499	–	10.219 ± 0.9	0.15 ± 0.02	73.01
LNC-2	$LaNi_4Co$	5.035	3.135	88.711 ± 0.8	0.09 ± 0.04	89.29
	$LaNi_5$	5.027	4.063	7.068 ± 1.3	0.14 ± 0.01	78.34
	Ni	3.498	–	3.384 ± 0.9	0.09 ± 0.03	70.09

Based on the diffraction patterns obtained, it can be seen that at the same intensity scales, the peaks in the diffraction pattern of the LNC-1 sample have significantly lower height compared to LNC-2, indicating a higher level of structural distortions and defects in the crystal lattice. Both samples exhibit peaks corresponding to the $LaNi_5$ phase with an expanded lattice parameter along the c-axis (a = 5.01430 Å, c = 3.97987 Å; PDF 04-008-6308). This phase is characterized by a high level of microstrain, which simultaneously leads to a reduction in peak intensity and broadening of the diffraction lines. The broadening of the diffraction peaks is determined by the combined contributions of the reduced average crystallite size and the presence of microstrains causing local distortions in the interplanar spacings [52–54].

Both samples also show the presence of a metallic Ni phase (a = 3.5285 Å; PDF 04-010-6148), characterized by reduced lattice parameters and relatively small crystallite sizes. The reduction in the lattice parameter of metallic Ni is attributed to internal stresses arising from mechanical milling, as well as to the size effect associated with the nanocrystalline structure [55].

The observed deviations in lattice parameters and the high microstrain values in the $LaNi_5$ and Ni phases indicate pronounced structural distortions associated with the formation of the intermetallic phase $LaNi_4Co$ during synthesis. Since the initial material was obtained by mechanical synthesis, the solid-state reaction process was accompanied by intense diffusion of Co atoms and their partial substitution of Ni atoms in the $LaNi_5$ phase structure [36].

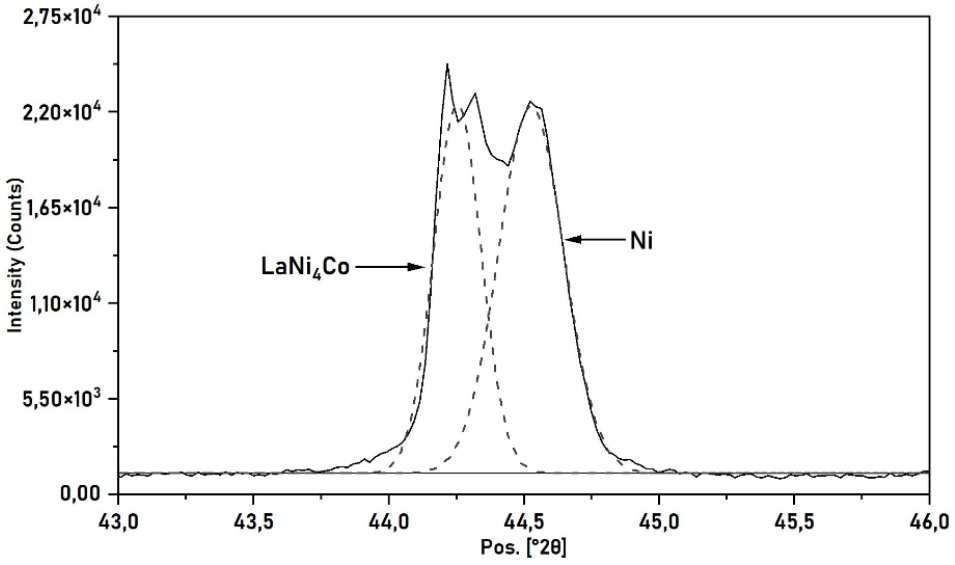

Figure 3. Approximation of overlapping Ni and $LaNi_4Co$ peaks around ~44° 2θ in sample LNC-1.

In all samples, overlapping diffraction peaks are observed near 44°, 52°, 75°, and 92° 2θ, corresponding to the Ni and $LaNi_4Co$ phases. This overlap is due to the close interplanar spacings of the crystallographic planes in these phases, causing them to be recorded at nearly the same angular positions when measured using Cu Kα radiation. To accurately distinguish individual phase contributions, Rietveld refinement of the profiles was performed, where the experimental data were approximated by a sum of model functions for each phase based on known crystallographic parameters. Figure 3 shows an example of peak fitting in the region around ~44° 2θ.

The experimental profile is clearly deconvoluted into components corresponding to the Ni and $LaNi_4Co$ phases, enabling a more precise assessment of their quantitative ratio and microstructural characteristics. This approach is standard in the analysis of multicomponent metallic and intermetallic systems where overlapping diffraction reflections occur [56,57].

The high mass fraction of $LaNi_4Co$ (Table 1) indicates that, during the interaction of the initial La, Ni, and Co powders, the most thermodynamically stable phase is the AB_5-type intermetallic compound with partial substitution of Ni by Co [58,59].

The low proportion of $LaNi_5$ reflects the ongoing substitution of Ni atoms by Co, leading to the formation of $LaNi_4Co$. This is accompanied by an increase in the lattice parameter c compared to the reference value, which may be related to the uneven distribution of Co and local lattice distortions. Such changes in lattice parameters are often interpreted as consequences of local redistribution of electron density and imperfect atomic packing during partial substitution [36]. Additionally, sample LNC-2 exhibits greater structural homogeneity and stability compared to LNC-1. This is manifested by a higher content of $LaNi_4Co$, a lower fraction of residual phases, reduced microstrains, and larger crystallite sizes in the $LaNi_5$ phase.

The resulting structure, where the primary phase is $LaNi_4Co$ and the amounts of residual $LaNi_5$ and Ni are minimized, is more resistant to both thermal and mechanical effects [35,36]. From the perspective of hydrogen storage technologies, such a combination of phases and microstructural characteristics can provide improved cyclic stability and resistance to degradation compared to pure $LaNi_5$, as supported by numerous experimental studies [35,36,39].

Hydrogen capacity and hydrogen absorption kinetics

The kinetics of hydrogen absorption and desorption are crucial parameters for the practical application of hydride alloys in hydrogen storage systems. Manometric measurement results showed that the addition of Co has a significant impact on both the hydrogen capacity and the kinetic characteristics of the $LaNi_5$ intermetallic system.

It should be noted that the PCT measurements were carried out at 100 °C, as this regime corresponds to the typical operating conditions of $LaNi_5$+Me-based alloys in hydrogen systems (80–120 °C), where an optimal balance between the hydrogen exchange rate and the equilibrium pressure is achieved. At temperatures of 80 °C and below, a significant slowdown of diffusion processes is observed, while at higher temperatures structural changes may occur, complicating the interpretation of the results. Therefore, a temperature of 100 °C was chosen as the most optimal condition for evaluating the working performance of the material.

For the initial $LaNi_5$, the theoretical hydrogen capacity is approximately 1.4 wt.% [23,24]. Figure 4 presents the pressure-composition isotherms (PCT) for samples LNC-1 and LNC-2.

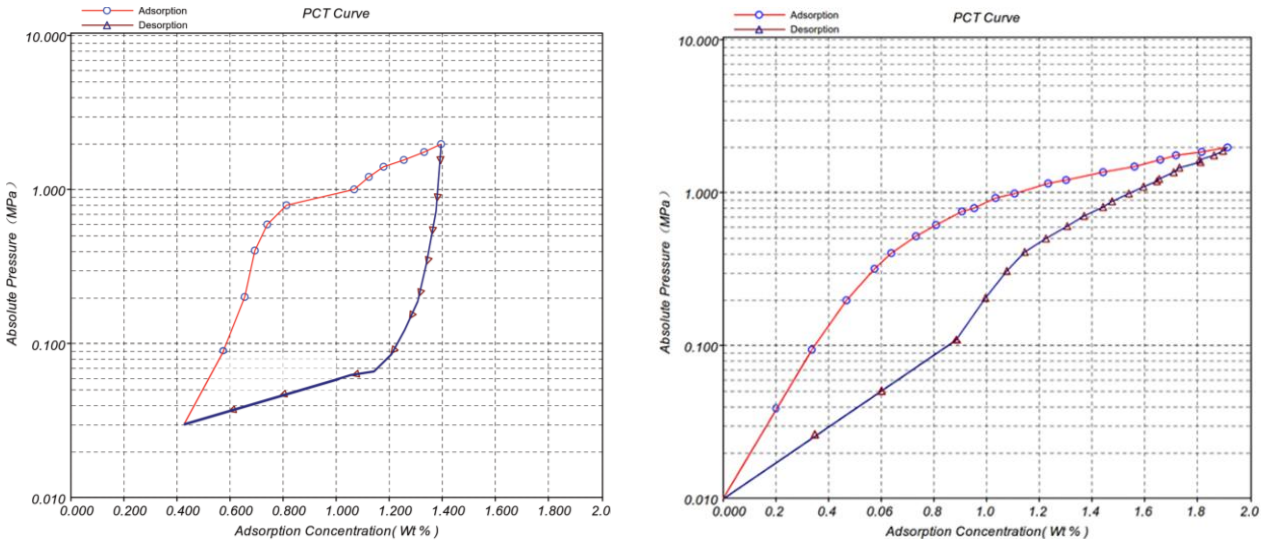

a) LNC-1 b) LNC-2

Figure 4. PCT curves of the studied samples obtained at 100 °C and a hydrogen pressure of 2 MPa.

In the initial section of the sorption isotherm of the LNC-1 sample (Figure 4a), a hydrogen content of approximately 0.4 wt.% is observed. This effect is attributed to the presence of residual hydrogen retained within interphase boundaries, crystal lattice defects, and nanopores after preliminary activation cycles. Even after high-temperature vacuum degassing, a small fraction of hydrogen may remain trapped in these structural inhomogeneities. This phenomenon is typical for $LaNi_5$-based alloys and does not affect the subsequent shape of the isotherm or the determination of thermodynamic parameters.

Sample LNC-1 reaches hydrogen saturation of approximately 1.4 wt.% H_2 at a pressure of around 1–2 MPa. Compared to pure $LaNi_5$, the maximum capacity is slightly lower; however, the material exhibits a pronounced plateau and a relatively stable hydride equilibrium region. The hysteresis between absorption and desorption processes is approximately 0.4–0.5 MPa, indicating moderate thermodynamic barriers during the reversible α↔β phase transition. The LNC-1 isotherm features a single-stage plateau without a distinct separation into multiple absorption stages.

Analysis of the dehydrogenation behavior of the LNC-2 sample shows that desorption proceeds less intensively, and the amount of released hydrogen in the pressure range of 2–0.1 MPa remains low, making it difficult to precisely determine the plateau position. The decrease in equilibrium pressure observed for LNC-2 indicates a more thermodynamically favorable dehydrogenation process and improved reversibility of the system. The LNC-2 sample exhibits a more pronounced hydrogen release and a reduced plateau pressure of approximately 0.18 MPa (compared to ~0.26 MPa for LNC-1), which is associated with the formation of additional desorption-active sites and a decrease in activation energy due to the substitution of nickel with cobalt. The experimentally observed maximum hydrogen capacity of ~1.9 wt.% exceeds the theoretical value for the classical $LaNi_5$ hydride (~1.5 wt.%). This effect can be explained by structural and electronic modifications of the crystal lattice induced by the partial substitution of nickel with cobalt, which promote the formation of additional hydrogen-binding sites, including defects, interphase boundaries, and internal cavities. The presence of secondary phases such as La_2Ni_7 or $LaNi_3$, which possess enhanced sorption capacity, also contributes significantly to

the overall hydrogen storage capacity. Collectively, these mechanisms account for the observed increase in capacity beyond the theoretical limit.

Kinetic measurements showed that Co modification significantly influences not only the equilibrium parameters but also the rates of hydrogen exchange processes. The addition of Co is known as an effective method to accelerate hydriding kinetics by reducing the reaction enthalpy and increasing the mobility of hydrogen atoms within the lattice [60]. The obtained sorption and desorption kinetic curves for samples LNC-1 and LNC-2 are presented in Figure 5.

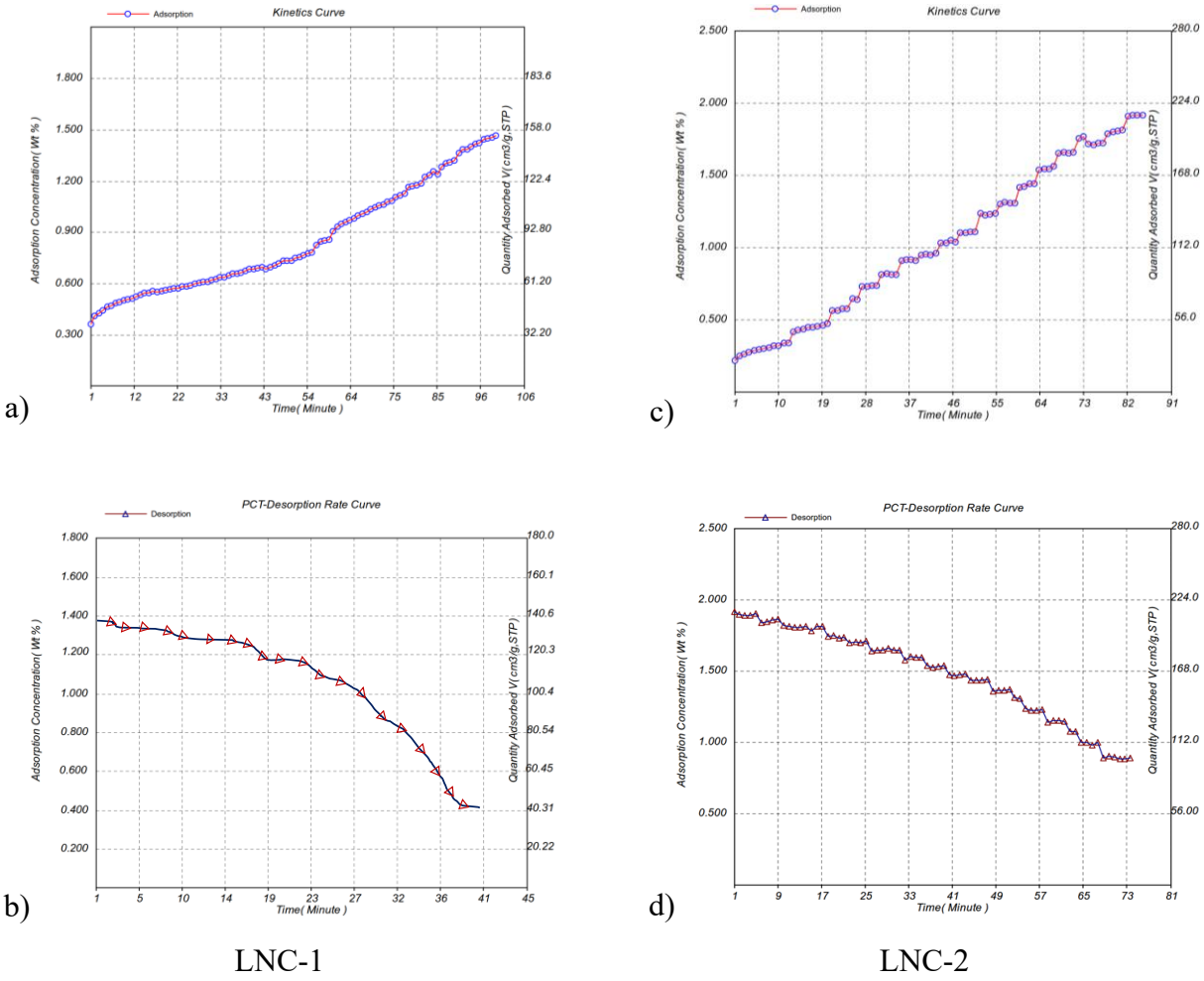

Figure 5. Hydrogen sorption (a, c) and desorption (b, d) kinetics curves for Co-modified $LaNi_5$ samples.

On the hydrogen absorption curves (Figure 5a, c), a gradual increase in hydrogen concentration over time is observed, followed by saturation. The process proceeds via a diffusion-limited mechanism and completes after approximately 90 minutes for both samples; however, the shapes of the curves differ. For the LNC-1 sample, the absorption process occurs more smoothly, with a lower initial sorption rate and a slightly reduced final capacity. In contrast, the LNC-2 sample exhibits more intense hydrogen uptake at the early stages and a higher ultimate capacity, which can be attributed to increased surface activity, a greater number of defects and interphase boundaries, and improved diffusion permeability resulting from the higher energy of the mechanosynthesis process. The mechanical

treatment conditions at a ball-to-powder ratio of 1:30 promote the formation of a fine-dispersed structure and an increased defect density, facilitating hydrogen diffusion into the particle bulk.

Hydrogen desorption (Figure 5b, d) is characterized by a gradual decrease in hydrogen content, and it should be noted that the process does not fully complete even after 73 minutes. This indicates the presence of strong hydrogen-binding centers and diffusion limitations on the release of hydrogen atoms. Nevertheless, for the LNC-2 sample, a more intense and uniform hydrogen release is observed throughout the entire experiment, confirming higher dehydrogenation activity, which is probably associated with a greater degree of structural defectiveness and an increased specific surface area. For LNC-1, the presence of a residual amount of hydrogen even at a low pressure of 0.1 MPa indicates more stable hydrogen retention in the lattice and lower reversibility of the hydride transformation.

A comparison of the results shows that an increase in the BPR during mechanical synthesis has a positive effect on the reaction kinetics: the initial absorption rate increases, the degree of dehydrogenation improves, and the system's reversibility is enhanced. More intensive mechanical alloying leads to the formation of submicron particles, an increase in the fraction of grain boundaries, and the creation of active sites for hydrogen diffusion. As a result, the sorption and desorption processes become more uniform and thermodynamically reversible [60–63].

The ball-to-powder ratio (BPR) determines the intensity of mechanical energy transfer to powder particles during milling, which directly affects the microstructural state of the material and, consequently, the kinetics of hydrogen interaction [64,65]. At a higher BPR (sample LNC-2), the frequency and energy of particle collisions increase, promoting not only a reduction in particle and crystallite sizes but also an increase in the density of structural defects. These defects, in turn, serve as additional diffusion channels and nucleation sites for the hydride phase. At a lower BPR (sample LNC-1), the milling process proceeds less intensively, leading to the formation of larger crystallites and a decrease in structural defect density, which consequently reduces the hydrogen absorption and desorption rates.

Therefore, both Co-substituted samples retain the hexagonal structure of the parent $LaNi_5$ but differ in kinetic and thermodynamic parameters: LNC-1 provides stable but slightly lower hydrogen storage capacity, while LNC-2 demonstrates enhanced kinetics, higher capacity, narrower hysteresis, and signs of a two-stage plateau, making it more promising for practical applications.

4. Conclusions

The results of this study demonstrate the influence of Co on the hydrogen absorption properties and phase composition of the intermetallic compound $LaNi_5$. It was established that cobalt modification in the $LaNi_5$ structure leads to the formation of a substitutional solid solution without the formation of new phases up to a Co concentration of $x \leq 1.5$. This is confirmed by X-ray phase analysis results, which reveal the preservation of the hexagonal AB_5-type structure. Minor changes in the lattice parameters were also observed, indicating partial substitution of Ni atoms by Co atoms. Such phase modifications contribute to the stabilization of the crystal lattice and improvement of the structural characteristics of the material.

In samples with Co addition ($LaNi_{5-x}Co_x$), a maximum hydrogen capacity of approximately 1.9 wt.% H_2 was achieved. This increase is attributed to the partial substitution of Ni by Co, which stabilizes the structure and facilitates hydrogen atom incorporation into the crystal lattice. Thus, Co modification

not only maintains a high specific capacity but also enables a slight increase in hydrogen storage at moderate pressures (~1–2 MPa).

Analysis of the kinetic curves revealed that both samples exhibit a diffusion-limited behavior; however, with more intensive mechanosynthesis, the initial absorption rate and dehydrogenation intensity increase. This effect is attributed to the higher fraction of interphase boundaries and the increased concentration of lattice defects. Thus, an increase in mechanosynthesis energy promotes the activation of hydrogen exchange and enhances the thermodynamic reversibility of hydride transformations, confirming the decisive role of microstructural factors in shaping the functional properties of $LaNi_5$-based alloys.

Use of AI tools declaration

The authors declare they have not used Artificial Intelligence (AI) tools in the creation of this article.

Acknowledgments

This work was financially supported by the Science Committee of the Ministry of Science and Higher Education of the Republic of Kazakhstan within the framework of the targeted funding program, project BR21882200 “Development and investigation of innovative technologies, materials, and devices for hydrogen production, storage and power generation”.

Conflicts of interest

The authors declare no conflicts of interest.

Author contributions

Conceptualization, I. Sokolov and N. Mukhamedova; methodology, O. Oken and M. Skopchenko; validation, N. Mukhamedova and A. Miniyazov; investigation, A. Nassyrova; writing – original draft preparation, N. Mukhamedova and A. Sabyrtayeva; writing – review and editing, M. Skakov and A. Miniyazov; project administration, M. Skakov.

References

1. Sahak MZM, Shaffee SNA, Thant MMM, et al. (2024) Advancement in green hydrogen production: Integrating Solid Oxide Electrolysis Cells (SOECs) into existing offshore facilities for sustainable energy. *Proceedings of the APOGCE 2024*, Perth, Australia, 15–17. https://doi.org/10.2118/221154-MS
2. Das HS, Chowdhury MFF, Li S, et al. (2021) Fuel cell and hydrogen power plants. *Hybrid Renewable Energy Syst Microgrids* 2021: 313–349. https://doi.org/10.1016/B978-0-12-821724-5.00009-X
3. Sikiru S, Oladosu TL, Amosa TI, et al. (2024) Hydrogen-powered horizons: Transformative technologies in clean energy generation, distribution, and storage for sustainable innovation. *Int J Hydrogen Energy* 56: 1152–1182. https://doi.org/10.1016/j.ijhydene.2023.12.186

4. Moradi R, Growth KM (2019) Hydrogen storage and delivery: Review of the state of the art technologies and risk and reliability analysis. *Int J Hydrogen Energy* 44: 12254–12269. https://doi.org/10.1016/j.ijhydene.2019.03.041
5. Sadeq AM (2024) Advances and challenges in hydrogen energy: A review. *Chem Eng Process Tech* 9: 1087. https://doi.org/10.47739/2333-6633/1087
6. Kyriakopoulos GL, Aravossis KG (2023) Literature review of hydrogen energy systems and renewable energy sources. *Energies* 16: 7493. https://doi.org/10.3390/en16227493
7. Federal Ministry for Economic Affairs and Climate Action (BMWK) (2023) National Hydrogen Strategy Update. Available from: https://www.bundeswirtschaftsministerium.de/Redaktion/EN/Publikationen/Energie/national-hydrogen-strategy-update.pdf?__blob=publicationFile&v=2.
8. New Energy and Industrial Technology Development Organization (NEDO) (2020) The world's largest-class hydrogen production, Fukushima Hydrogen Energy Research Field (FH2R) now is completed at Namie town in Fukushima. Available from: https://www.nedo.go.jp/english/news/AA5en_100422.html.
9. Energy Innovation Austria (2020) H2FUTURE, Green hydrogen pilot plant at industrial scal. Available from: https://www.energy-innovation-austria.at/article/h2future-2/?lang=en.
10. Kempler PA, Slack JJ, Baker AM (2022) Research priorities for seasonal energy storage using electrolyzers and fuel cells. *Joule* 6: 280–285. https://doi.org/10.1016/j.joule.2021.12.020
11. Petkov I, Gabrielli P (2020) Power-to-hydrogen as seasonal energy storage: An uncertainty analysis for optimal design of low-carbon multi-energy systems. *Appl Energy* 274: 115197. https://doi.org/10.1016/j.apenergy.2020.115197
12. Kwon K, Lee HB, Kim N, et al. (2024) Integrated battery and hydrogen energy storage for enhanced grid power savings and green hydrogen utilization. *Appl Sci* 14: 7631. https://doi.org/10.3390/app14177631
13. Sun W, Vasu S, Blais MS (2022) Chapter 2—Fundamentals. *Machinery and Energy Systems for the Hydrogen Economy*, Elsevier, 11–30. https://doi.org/10.1016/B978-0-323-90394-3.00015-1
14. Ball M, Wietschel M (2009) The future of hydrogen—Opportunities and challenges. *Int J Hydrogen Energy* 34: 615–627. https://doi.org/10.1016/j.ijhydene.2008.11.014
15. Züttel A (2003) Materials for hydrogen storag. *Mat Today* 6: 24–33. https://doi.org/10.1016/S1369-7021(03)00922-2
16. Schlapbach L, Züttel A (2001) Hydrogen-storage materials for mobile applications. *Nature* 414: 353–358. https://doi.org/10.1038/35104634
17. Züttel A (2004) Hydrogen storage methods. *Naturwissenschaften* 91: 157–172. https://doi.org/10.1007/s00114-004-0516-x
18. Jain IP, Lal C, Jain A (2010) Hydrogen storage in Mg: A most promising material. *Int J Hydrogen Energy* 35: 5133–5144. https://doi.org/10.1016/j.ijhydene.2009.08.088
19. Nemukula E, Mtshali CB, Nemangwele F (2025) Metal hydrides for sustainable hydrogen storage: A review. *Int J Energy Res*. https://doi.org/10.1155/er/6300225
20. Bowman RC, Fultz B (2022) Metallic hydrides I: Hydrogen storage and other gas-phase applications. *Bulletin Mat Res Soc* 27: 688–693. https://doi.org/10.1557/MRS2002.223
21. Martin M, Gommel C, Borkhart C, et al. (1996) Absorption and desorption kinetics of hydrogen storage alloys. *J Alloys Compd* 238: 193–201. https://doi.org/10.1016/0925-8388(96)02217-7

22. Dematteis EM, Barale J, Corno M, et al. (2021) Solid-state hydrogen storage systems and the relevance of a gender perspective. *Energies* 14: 6158. https://doi.org/10.3390/en14196158
23. Luo S, Clewley JD, Flanagan TB, et al. (1998) Further studies of the isotherms of $LaNi_{5-x}Sn_x$–H for x = 0–0.5. *J Alloys Compd* 267: 171–181. https://doi.org/10.1016/S0925-8388(97)00536-7
24. Luo S, Clewley JD, Flanagan TB, et al. (1997) Split plateaux in the $LaNi_5$–H system and the effect of Sn substitution on splitting. *J Alloys Compd* 253–254: 226–231. https://doi.org/10.1016/S0925-8388(96)02904-0
25. Du H, Zhang W, Wang C, et al. (2003) Neutron powder diffraction study on the structures of $LaNi_{5-x}A1_xD_y$ compounds. *Solid State Commun* 128: 157–161. https://doi.org/10.1016/S0038-1098(03)00655-0
26. Liu J, Li K, Cheng H, et al. (2017) New insights into the hydrogen storage performance degradation and Al functioning mechanism of $LaNi_{5-x}Al_x$ alloys. *Int J Hydrogen Energy* 42: 24904–24914. https://doi.org/10.1016/j.ijhydene.2017.07.213
27. Zhu S, Chen X, Liu J, et al. (2020). Long-term hydrogen absorption/desorption properties of an AB_5-type $LaNi_{4.75}Mn_{0.25}$ alloy. *Mat Sci Eng B* 262: 114777. https://doi.org/10.1016/j.mseb.2020.114777
28. Almeida Neto GR de, Gonçalves Beatrice CA, Leiva DR, et al. (2021) Polyetherimide-$LaNi_5$ composite films for hydrogen storage applications. *Int J Hydrogen Energy* 46: 23767–23778. https://doi.org/10.1016/j.ijhydene.2021.04.191
29. Kodama T (1999) The thermodynamic parameters for the $LaNi_{5-x}Al_x$–H_2 and $MmNi_{5-x}Al_x$–H_2 systems. *J Alloys Compd* 289: 207–212. https://doi.org/10.1016/s0925-8388(99)00173-5
30. Nakamura Y, Akiba E (2002) Defects formation in $LaNi_5$-based alloys investigated by In-situ X-ray diffraction. *MRS Proceed*, 753. https://doi.org/10.1557/proc-753-bb5.56
31. Huang T, Yu H (1989) An X-ray diffraction study on phase transition lattice gas in $LaNi_5H_x$. *J Less-Common Me* 153: 253–257. https://doi.org/10.1016/0022-5088(89)90119-7
32. Chen J, Dou SX, Liu HK (1996) Effect of partial substitution of La with Ce, Pr and Nd on the properties of $LaNi_5$-based alloy electrodes. *J Power Sources* 63: 267–270. https://doi.org/10.1016/s0378-7753(96)02461-5
33. Todorova S, Abrashev B, Rangelova V, et al. (2021) Hydrogen gas phase and electrochemical hydriding of $LaNi_{5-x}M_x$ (M = Sn, Co, Al) alloys. *Materials* 14: 14. https://doi.org/10.3390/ma14010014
34. Souza EC, Ticianelli EA (2003) Effect of partial substitution of nickel by tin, aluminum, manganese and palladium on the properties of $LaNi_5$-type metal hydride alloys. *J Braz Chem Soc*, 14. https://doi.org/10.1590/S0103-50532003000400009
35. Liu J, Zhu S, Zheng Z, et al. (2019) Long-term hydrogen absorption/desorption properties and structural changes of $LaNi_4Co$ alloy with double desorption plateaus. *J Alloys Compd* 778: 681–690. https://doi.org/10.1016/j.jallcom.2018.11.164
36. Zhu Z, Zhu S, Lu H, et al. (2019) Stability of $LaNi_{5-x}Co_x$ alloys cycled in hydrogen—Part 1 evolution in gaseous hydrogen storage performance. *Int J Hydrogen Energ* 44: 15159–15172. https://doi.org/10.1016/j.ijhydene.2019.04.111
37. Belkhiria S, Alsawi A, Hraiech I, et al. (2024) Experimental and mathematical investigation of hydrogen absorption in $LaNi_5$ and $La_{0.7}Ce_{0.1}Ga_{0.3}Ni_5$ compounds. *Metals* 14: 967. https://doi.org/10.3390/met14090967

38. Lys A, Fadonougbo JO, Faisal M, et al. (2020) Enhancing the hydrogen storage properties of A_xB_y intermetallic compounds by partial substitution: A short review. *Hydrogen* 1: 38–63. https://doi.org/10.3390/hydrogen1010004
39. Sato T, Ikeda K, Honda T, et al. (2022) Effect of Co-substitution on hydrogen absorption and desorption reactions of $YMgNi_4$-based alloy. *J Phys Chem* 126. https://doi.org/10.1021/acs.jpcc.2c03265
40. Liang G, Huot J, Schulz R (2001) Hydrogen storage properties of the mechanically alloyed $LaNi_5$-based materials. *J Alloys Compd* 320: 133–139. https://doi.org/10.1016/S0925-8388(01)00929-X
41. Skakov M, Miniyazov A, Tulenbergenov T, et al. (2024) Hydrogen production by methane pyrolysis in the microwave discharge plasma. *AIMS Energy* 12: 548–560. https://doi.org/10.3934/energy.2024026
42. Miniyazov A, Skakov M, Tulenbergenov T, et al. (2025) Structural evolution of carbon from methane pyrolysis in microwave plasma. *Carb Trends* 21: 100552. https://doi.org/10.1016/j.cartre.2025.100552
43. Skakov M, Kozhakhmetov Ye, Mukhamedova N, et al. (2022) Effect of a High-Temperature Treatment on Structural-Phase State and Mechanical Properties of IMC of the Ti-25Al-25Nb at.% System. *Materials* 15: 5560. https://doi.org/10.3390/ma15165560
44. Mukhamedova NM, Miniyazov AZ, Zhanbolatova GK, et al. (2025) Evolution of phase transformations in the Mg-Ni-Ce system after mechanical synthesis and spark plasma sintering. *Materials* 18: 2131. https://doi.org/10.3390/ma18092131
45. Mukhamedova N, Miniyazov A, Sabyrtayeva A, et al. (2025) Dispersion of sintered Mg-Ni-Ce materials for efficient hydrogen storage. *Crystals* 15: 743. https://doi.org/10.3390/cryst15080743
46. Miniyazov A, Skakov M, Mukhamedova N, et al. (2025) Structural and phase characteristics of $LaNi_5$-based materials modified with Ti, Mn, and Co. *Alloys* 4: 25. https://doi.org/10.3390/alloys4040025
47. Malik S, Zhigalenok Y, Skakov M, et al. (2025) Nano- and micro-sized $LaNi_5$ electrochemical behaviour as anode material for Ni–MH batteries. *Eur Chem-Tech J* 27: 13–20. https://doi.org/10.18321/ectj1652
48. Malik S, Zhumadil K, Avchukir K, et al. (2025) Enhancing electrochemical performance of $LaNi_5$ anodes using MXene as a multifunctional additive for Ni-MH batteries. *J Electroanal Chem* 996: 119409. https://doi.org/10.1016/j.jelechem.2025.119409
49. International Centre for Diffraction Data (ICDD). PDF-4 Axiom, 2025; ICDD: Newtown Square, PA, USA. Available from: https://www.icdd.com/pdf-4-axiom/.
50. Olivero JJ, Longbothum RL (1977) Empirical fits to the Voigt line width: A brief review. *J Quant Spectrosc Radiat Transfer* 17: 233–236. https://doi.org/10.1016/0022-4073(77)90161-3
51. Rietveld HM (1969) A profile refinement method for nuclear and magnetic structures. *J Appl Cryst* 2: 65–71. https://doi.org/10.1107/S0021889869006558
52. Williamson GK, Hall WH (1953) X Ray line broadening from filed aluminium and wolfram. *Acta Metall* 1: 22–31. https://doi.org/10.1016/0001-6160(53)90006-6
53. Nakamura Y, Akiba E (2000). In-situ X-ray diffraction study on $LaNi_5$ and $LaNi_{4.75}Al_{0.25}$ in the initial activation process. *J Alloys Compd* 308: 309–318. https://doi.org/10.1016/s0925-8388(00)01033-1

54. Noroozi AH, Safa S, Azimirad R, et al. (2012) Microstructure and hydrogen storage properties of $LaNi_5$-Multi Wall Carbon Nanotubes (MWCNTs) composite. *Arabian J Sci Eng* 38: 187–194. https://doi.org/10.1007/s13369-012-0414-z
55. Deb AK, Chatterjee P (2019) Study of deformation microstructure of nickel samples at very short milling times: effects of addition of α-Al_2O_3 particles. *J Theor Appl Phys*, 13. https://doi.org/10.1007/s40094-019-0319-2
56. Rodríguez-Carvajal J (1993) Recent advances in magnetic structure determination by neutron powder diffraction. *Phys B* 192: 55–69. https://doi.org/10.1016/0921-4526(93)90108-I
57. Toby BH (2006) *R* factors in Rietveld analysis: How good is good enough? *Powder Diffr* 21: 67–70. https://doi.org/10.1154/1.2179804
58. Chartouni D, Meli F, Züttel A, et al. (1996) The influence of cobalt on the electrochemical cycling stability of $LaNi_5$-based hydride forming alloys. *J Alloys Compd* 241: 160–166. https://doi.org/10.1016/0925-8388(96)02331-6
59. Khaldi C, Mathlouthi H, Lamloumi J, et al. (2004) Electrochemical study of cobalt-free AB_5-type hydrogen storage alloys. *Int J Hydrogen Energy* 29: 307–311. https://doi.org/10.1016/s0360-3199(03)00157-5
60. Akiba E, Iba H (1998) Hydrogen absorption by $LaNi_5$-based alloys substituted with various transition metals. *Intermetallics* 6: 461–470 https://doi.org/10.1016/S0966-9795(97)00088-5
61. Sakintuna B, Lamari-Darkrim F, Hirscher M (2007) Metal hydride materials for solid hydrogen storage: A review. *Int J Hydrogen Energy* 32: 1121–1140. https://doi.org/10.1016/j.ijhydene.2006.11.022
62. Lototskyy MV, Davids MW, Tolj I, et al. (2015) Metal hydride systems for hydrogen storage and supply for stationary and automotive low temperature PEM fuel cell power modules. *Int J Hydrogen Energy* 39: 9879–9888. https://doi.org/10.1016/j.ijhydene.2015.01.095
63. Gao ZJ, Luo YC, Lin Z, et al. (2003) Effect of Co substitution for Ni on the microstructure and electrochemical properties of La-R-Mg-Ni-based hydrogen storage alloys. *J Solid State Electrochem* 17: 727–735. https://doi.org/10.1007/s10008-012-1878-1
64. Suryanarayana C (2004) Mechanical alloying and milling (1st Edition). CRC Press: Boca Raton, FL, USA. https://doi.org/10.1201/9780203020647
65. Whang SH (2011) Nanostructured metals and alloys: Processing, microstructure, mechanical properties and applications. Woodhead Publishing: Cambridge, UK. Available from: https://pdfs.semanticscholar.org/f5f4/49e94df44c2f510c5f3f08cd16e0a9f01c42.pdf.